LAWRENCE
LIVERMORE
NATIONAL
LABORATORY

LLNL-TR-435981

# The prediction of Neutron Elastic Scattering from Tritium for E(n) = 6-14 MeV

J. D. Anderson, F. S. Dietrich, T. Luu, D. P. McNabb, P. Navratil, S. Quaglioni

June 16, 2010

## Disclaimer



This work performed under the auspices of the U.S. Department of Energy by Lawrence Livermore National Laboratory under Contract DE-AC52-07NA27344.

# THE PREDICTION OF NEUTRON ELASTIC SCATTERING FROM TRITIUM FOR $E_n$ = 6-14 MeV

J. D. Anderson, F. S. Dietrich, T. Luu, D. P. McNabb, P. Navratil, S. Quaglioni
Lawrence Livermore National Laboratory
P.O. Box 808, Livermore, CA 94551

June 14, 2010

## Abstract

In a recent report Navratil *et al*. [1] evaluated the angle-integrated cross section and the angular distribution for 14-MeV n+T elastic scattering by inferring these cross sections from accurately measured p+$^3$He angular distributions. This evaluation used a combination of two theoretical treatments, based on the no-core shell model and resonating-group method (NCSM/RGM) [2] and on the R-matrix formalism [3], to connect the two charge-symmetric reactions n+T and p+$^3$He. In this report we extend this treatment to cover the neutron incident energy range 6-14 MeV. To do this, we evaluate angle-dependent correction factors for the NCSM/RGM calculations so that they agree with the p+$^3$He data near 6 MeV, and using the results found earlier near 14 MeV we interpolate these correction factors to obtain correction factors throughout the 6-14 MeV energy range. The agreement between the corrected NCSM/RGM and R-Matrix values for the integral elastic cross sections is excellent (±1%), and these are in very good agreement with total cross section experiments. This result can be attributed to the nearly constant correction factors at forward angles, and to the evidently satisfactory physics content of the two calculations. The difference in angular shape, obtained by comparing values of the scattering probability distribution P($\mu$) vs. $\mu$ (the cosine of the c.m. scattering angle), is about ±4% and appears to be related to differences in the two theoretical calculations. Averaging the calculations yields P($\mu$) values with errors of ±2½% or less. These averaged values, along with the corresponding quantities for the differential cross sections, will form the basis of a new evaluation of n+T elastic scattering. Computer files of the results discussed in this report will be supplied upon request.

## I. Introduction

The physical principles involved in the use of a charge conjugate reaction to determine neutron cross sections from charged-particle data were discussed as early as 1966 by Anderson and Lutz [4]. Very recently, Navratil *et al*. [1] used such principles to determine cross sections for n+T at 14-MeV incident energy from measured values for p+$^3$He at a nearby energy (13.6 MeV). In that work, the physics content was provided by using a no-core shell model (NCSM) for the structure of the mass-3 systems, together with a resonating-group method (RGM) calculation to describe the interaction with the projectile. Because of the missing treatment of the three-body breakup of the tritium target, the calculations do not exactly describe the behavior of the angular distributions. Therefore, this approach used an angle-dependent correction factor (CF) generated by fitting the calculated elastic scattering to the experimental values for p+$^3$He at 13.6 MeV. The same correction factor was then used in the determination of the angular distribution for n+T from the NCSM/RGM calculations at 14 MeV. Comparisons were made with the results of R-matrix calculations [3], which were also used to infer n+T cross sections from p+$^3$He measurements, with generally satisfactory results.

In this report, the technique is extended to lower energies (6-14 MeV). Some physics judgment is used, but basically only simple numerical procedures are used in generating CF's. As in the 14-MeV case, the CF's are then applied to the uncorrected NCSM/RGM calculations to determine the appropriate n+T elastic differential cross sections.

The numerical NCSM/RGM results in the neutron-energy range from 6 to 14 MeV were obtained by P. Navratil as described in Ref. [1] using the LC machines. These results were subsequently tabulated to facilitate further manipulations. The calculated R-matrix cross sections were taken from the ENDL library, which in turn were derived from the entries in ENDF/B-VII. Because of the fact that many of the calculations that follow were performed by spreadsheet programs, it was necessary to choose entries from the tabulated NCSM/RGM and R-matrix cross sections that could be easily handled. The results from both calculations are presented as a function of incident energy and angle (or, equivalently, the cosine of the c.m. scattering angle $\mu$). Specifically, we required the cross sections at all energies to be available on a common evenly-spaced grid in $\mu$. The angular distributions we used,

represented by probability functions P($\mu$), were characterized by 33 equally spaced entries in $\mu$; *i. e.*, $\Delta\mu = 0.0625$. This allowed integration by simply summing entries (that is, a trapezoidal integration). Choosing only the data on this grid is a significant truncation of the available data set. In some cases linear interpolations between tabulated angles were required. Numerical checks show that no errors in any of the estimated quantities resulting from these truncations and interpolations exceed 1%.

Unless otherwise stated, incident neutron energies are in the laboratory system, and the scattering angles, $\mu$ values, and differential cross sections are center-of-mass quantities.

## II. Correction Factors

We begin by generating a CF at 14 MeV in a way similar to what was done in Navratil *et al*. [1], but with some minor variations. Previously we used CF's for p+$^3$He at the same bombarding energy as in the n+T calculation. As noted in Ref. [3], Hale in his R-matrix calculations adjusted the energy scale between incident protons and neutrons by a constant that approximates the Coulomb displacement energy (the estimate of the energy offset caused by the Coulomb force inside the nucleus). What we really want to do is to compare proton and neutron data at energies where the nuclear phase shift caused by the potential is the same in the two cases. Because of the presence of the Coulomb amplitude we can never really achieve this goal, but we know that the best correspondence will be for $E_p$ larger than $E_n$. However, we expect the difference to be less than the Coulomb displacement energy.

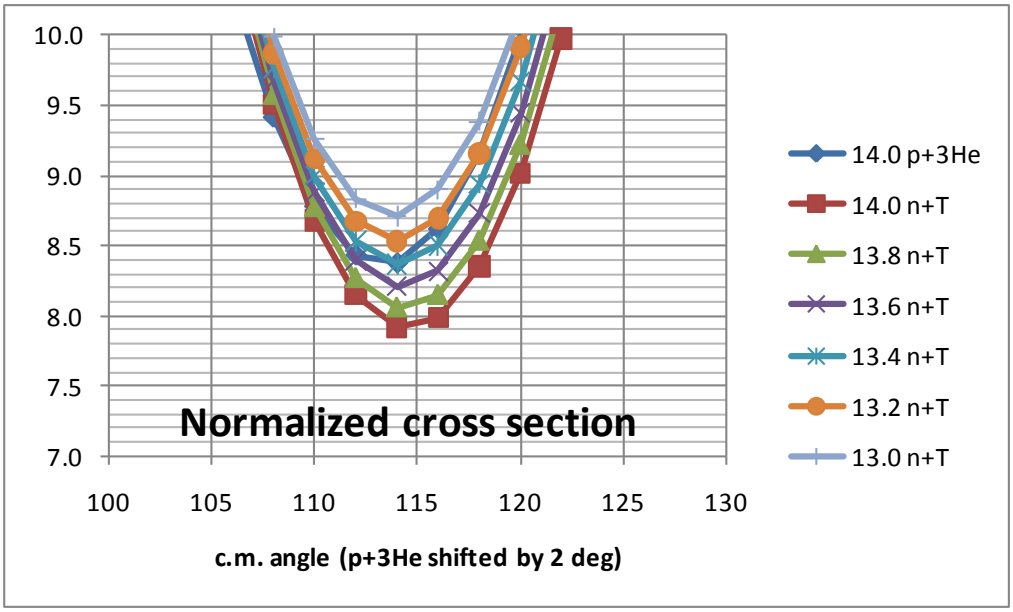


**Figure 1. The angular distribution of the calculated n+T elastic scattering cross section is plotted near the minimum at 114°, normalized to the 14 MeV cross section. Also shown is the calculated p+$^3$He cross section at 14 MeV shifted by 2° toward smaller angles.**

We attempt to estimate this shift by comparing value of the cross section at the minima in the n+T elastic angular distributions with those from the p+$^3$He angular distributions in the vicinity of 14 MeV bombarding energy, using the NCSM/RGM calculations. The absolute cross sections for the n+T

data are scaled to give the same angle-integrated cross section as the 14 MeV values, since we know that the angle-integrated n+T cross section increases by 7.5% in going from 14 to 13 MeV. In Figure 1 we show these data for n+T at several energies in the 13-14 MeV range, and at 14 MeV only for p+$^3$He. The p+$^3$He cross sections have been shifted to lower angles by 2°, so that the minimum is at the same angle in both reactions. From the figure we see that the behavior near the minimum is similar for p+$^3$He at 14 MeV and n+T at 13.4 MeV. It is clear that this 600-keV laboratory-energy shift is significantly smaller than the Coulomb displacement energy of 850 keV used by Hale [3], which corresponds to a difference of 1.1 MeV in the laboratory system. Other simple attempts to determine an energy shift, including solving a potential model with and without a Coulomb potential, suggest values for the shift within a few hundred keV of the procedure described above. We choose a laboratory-energy shift of 900 keV. The uncertainty in this value is not very important, since the correction factors are rather insensitive to the value of the shift. For example, to determine the CF's for n+T at 14 MeV, we find that using proton energies of either 14.6 or 15.1 MeV in the p+$^3$He mirror reaction gives correction factors (CF) which differ from those using the 14.9 MeV value by less than 0.5%.

In Figure 2 we plot the ratio of the p+$^3$He experimental data divided by the NCSM/RGM calculation for $E_p$ = 13.6 and 16.23 MeV. The data are from Hutson *et al*. [5]. We construct a CF for 14-

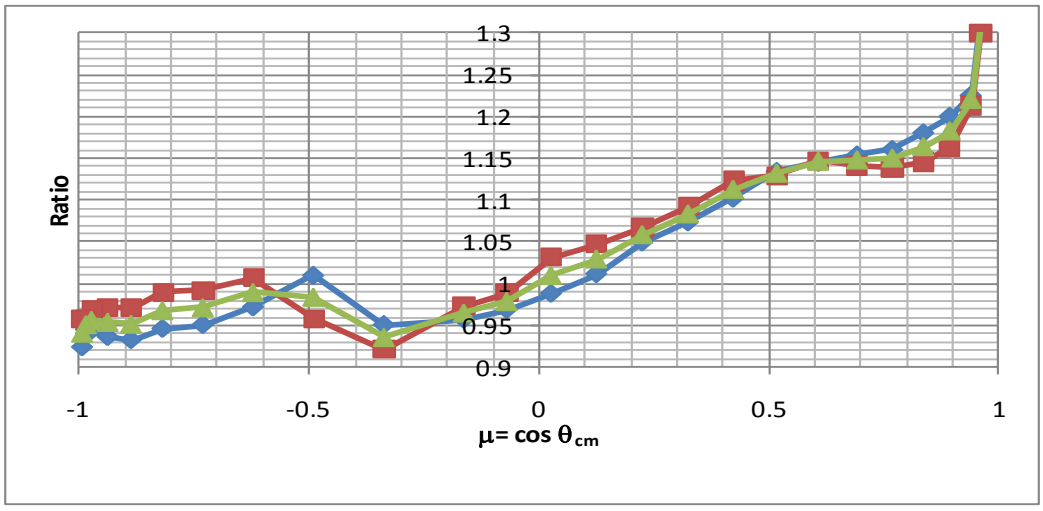


**Figure 2. The CF (correction factor) derived by dividing the measured p+$^3$He cross section by the NCSM/RGM calculation of Navratil and Quaglioni [2] is shown for $E_p$=13.6 MeV (red curve) and $E_p$=16.23 MeV (blue curve). Also shown is the constructed CF for a proton energy of 14.9 MeV (green curve), which corresponds to an n+T incident energy of 14 MeV.**

MeV neutrons by simply making a linear interpolation between the two data sets. Since we want a shifted proton bombarding energy of 14.9 MeV, this is simply 0.5 $CF_{13.6}$ + 0.5 $CF_{16.2}$. The constructed CF for 14 MeV neutrons is also shown in Figure 2.

For lower energies there is a paucity of high quality (errors <1%) data for p+$^3$He. For example, the data of McDonald *et al*. [6] at $E_p$ = 6.82, 8.82 and 10.77 MeV have errors larger than 2%. Thus a different approach is needed. In Navratil *et al*. [1] there is a comparison of Hale's R-matrix approach at 6 MeV with the calculations of Viviani *et al*. [7] at the same energy. The Viviani *et al*. calculation may be viewed as a more complete variant of the NCSM/RGM calculations used here, which is facilitated by

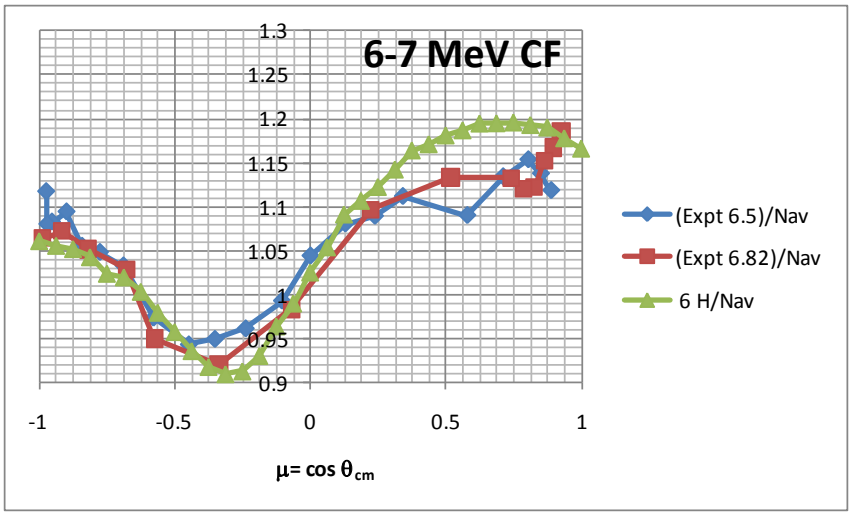


**Figure 3. The 6 MeV n+T R-matrix cross section of Hale divided by the calculated n+T NCSM/RGM cross section of Navratil and Quaglioni [2] is shown (labeled H/Nav). This should approximate an effective CF. Also shown are CF values obtained by dividing p+$^3$He experimental data with the NCSM/RGM calculations for $E_p$=6.5 and 6.82 MeV.**

the lower bombarding energy. Since Hale's R-matrix calculations and those of Viviani *et al*. agree almost exactly on the angular distributions, and since they also reproduce the experimental angle-integrated elastic cross section, we choose to construct a CF at 6 MeV by calculating the ratio of the R-matrix to NCSM/RGM calculations at that energy. The assumptions we make are that the corrected NCSM/RGM calculation should be equal to that of Viviani *et al*., and that the Viviani *et al*. and R-matrix calculations correctly predict the angular distribution as well as the angle-integrated cross section. The results for the CF are shown in Figure 3. The rise at the back angles (μ in the vicinity of -1) is consistent with the $E_p$ = 5.5 MeV proton data [8] so we plot the CF determined by using the McDonald *et al*. 6.82 MeV data [6] divided by the NCSM/RGM p+$^3$He calculation. Remembering that there are 2% errors on

the data, this would appear to validate the CF determined for n+T for angles larger than approximately 75°. In determining the CF's in this energy range, we have used the same 900-keV shift between incident neutron and proton energies as in the 14-MeV region.

The forward angles present a problem. At extremely low angles (less than 20°) does the CF bend over as suggested by Figure 3 or continue to rise as suggested by Figure 2, or is it flat? Here we reverted to an algorithm developed in 1958 [9] to fit 14 MeV neutron elastic scattering from light nuclei. It states that the log of the elastic cross section, plotted versus the cosine of the c.m. scattering angle, is a straight line. This was found to be true for $^{6}$Li, $^{7}$Li, Be, C, N and O. It also fits Hale's R-matrix 14 MeV calculation. By comparing the result of multiplying the NCSM/RGM calculation by various shapes for the correction factor for angles less than 20° it was obvious that neither of the extreme versions (*i. e.*, the bending over or the rise) produced a straight line on a log plot for the resultant n+T cross section. The largest acceptable deviations from the straight-line form were assumed to be a few percent (<5%) from 30° to 0°. The flat behavior of the CF is consistent with this criterion. In the absence of a definitive solution to this problem, we have chosen to proceed using the assumption that the CF at low angles is almost flat. In our actual CF's, we will allow a slight downward bend toward 0°.

If we pay attention to the low-angle p+$^{3}$He data (less than 60°, corresponding to $\mu$>0.5), there seems to be a slight variation with energy in the magnitude of the CF's, which we are assuming are approximately flat in this angular range. The magnitudes of the CF's in the forward-angle region of the two p+$^{3}$He data sets at 9.5 MeV [8] and 10.7 MeV [6], determined by comparing with the NCSM/RGM p+$^{3}$He calculations, are approximately 2% lower than those for the 13.6 and 16.2 MeV data [5]. Also, the angular average of the CF at forward angles from the 6-MeV n+T R-matrix vs. NCSM/RGM comparison is almost 4% larger than that in the 14-MeV region. We therefore adjust the magnitude of the forward CF downward by 0.5% per MeV from 14 MeV to 10 MeV, and then upward at 1% per MeV from 10 MeV to 6 MeV. The net adjustment (relative to 14 Mev) of +2% at 6 MeV turns out to be a good compromise between a rough average value of the results for p+$^{3}$He in the 6-6.9 MeV region and the +4% from the comparison of n+T data using the ratio of R-matrix to NCSM/RGM calculations. The actual CF's that we generated at 6 and 14 MeV, and which we use as the basis for interpolation to other energies, are shown in Figure 4.

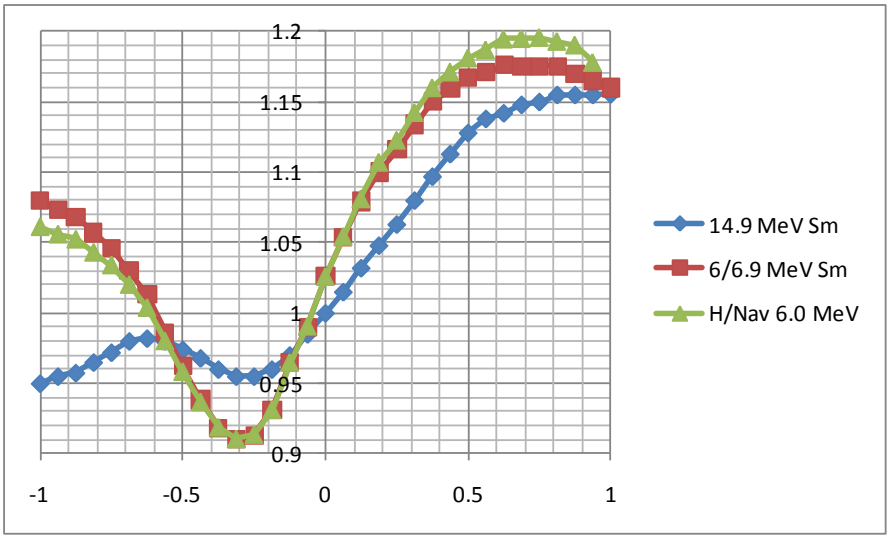


**Figure 4. The red and blue curves show the final CF's, smoothed and energy shifted, which were used with a linear algorithm to generate CF's from 6-14MeV are shown vs. μ, the cosine of the c.m. scattering angle. The CF at 6 MeV obtained directly from the R-matrix to NCSM/RGM ratio for n+T is also shown (green curve, labeled H/Nav).**

We can now specify the procedure used to determine the CF at an arbitrary energy in the 6-14 MeV range. For angles away from the forward region (*i. e.*, for $\mu < 0.5$) we use a linear interpolation in energy based on our constructed 14 MeV CF (derived at a p+$^3$He energy of 14.9 MeV) and our 6 MeV CF (based on the R-matrix to NCSM/RGM ratio). At forward angles ($\mu > 0.5$) we use the energy-dependent but nearly angle-independent values for the CF's described in the last paragraph, and shown by the curves labeled "Sm" in Figure 4. We use a linear energy interpolation in the forward region, also. The sharp structure caused by this algorithm in the region around $\mu = 0.5$ is smoothed by using an averaging over 5 steps in $\mu$; that is, $\{CF(\mu_n)\}_{av} = [¼CF(\mu_{n-2})+½CF(\mu_{n-1}) + CF(\mu_n) + ½CF(\mu_{n+1}) + ¼CF(\mu_{n+2})]/2.5$. An *a posteriori* justification for the use of the chosen method for interpolation is that the resultant angle-integrated elastic cross sections are in agreement with the R-matrix results to approximately 1% (see Table 3 in the Appendix).

Examples of the resultant CF's are shown in Figure 5. All CF's, in 1-MeV steps from 6 to 14 MeV, are shown in Figure A1 in the Appendix.

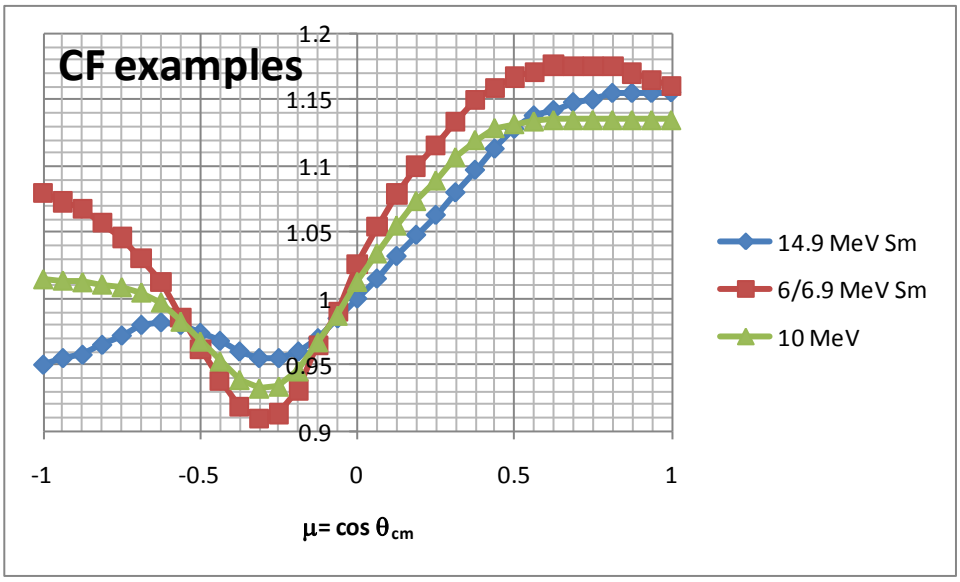


**Figure 5. Examples of CF's used in calculations of n+T cross sections are shown. The complete set is displayed in the Appendix, Figure A1.**

## III. Calculated n+T Cross Sections

After determining the correction factors, the NCSM/RGM calculations were then multiplied by the appropriate CF's to generate differential cross sections. Examples are shown in Figure 6, and the entire data set is tabulated in Table 1 in the Appendix and plotted as Figure A2. These differential cross sections were also averaged with those from the ENDF/B-VII R-matrix evaluation, and the results are shown in Table 2. The averaging procedure and final uncertainty estimates are discussed at the end of this section.

The results of integrating the corrected NCSM/RGM cross sections over solid angle gave 1983 mb at 6MeV, 1331 mb at 10MeV, and 947 mb at 14MeV. These are in very good agreement with Hale's R-matrix values of 2008mb, 1325mb and 940mb, respectively. The values for all energies are given in Table 3 in the Appendix.

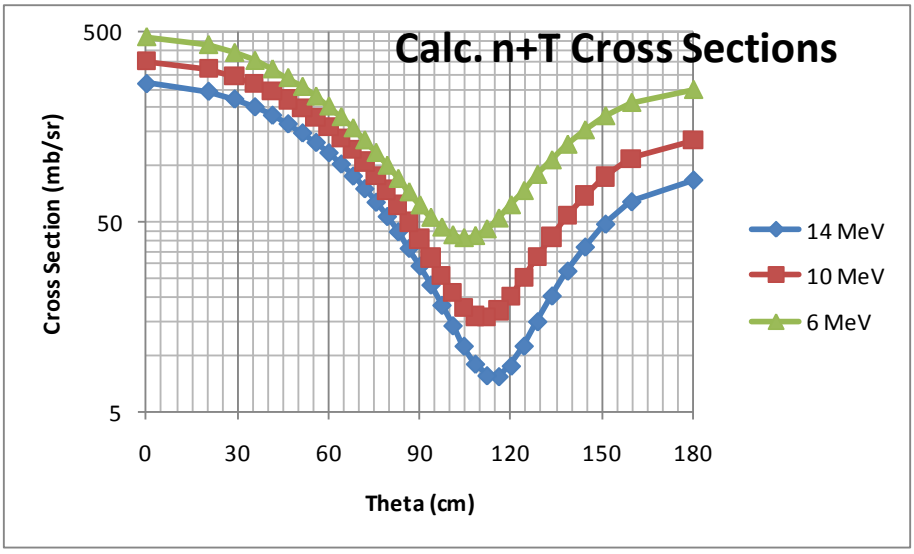


**Figure 6. Examples of calculated n+T elastic scattering cross sections for 6, 10 and 14 MeV are plotted as a function of center of mass angle. The complete set is shown in the Appendix, Figure A2. The cross sections are in mb/sr.**

Using the calculated angular distributions we can also derive the probability distributions P(μ). These are defined so that the integral of P(μ) over μ, the cosine of the scattering angle, is unity. The P(μ) values determined from the corrected NCSM/RGM calculations are slightly different from those gotten from the R-matrix calculations. We have plotted the ratio of P(μ) values given by the two calculations for several energies in Figure 7. The ratios for all energies are shown in the Appendix, Figure A3.

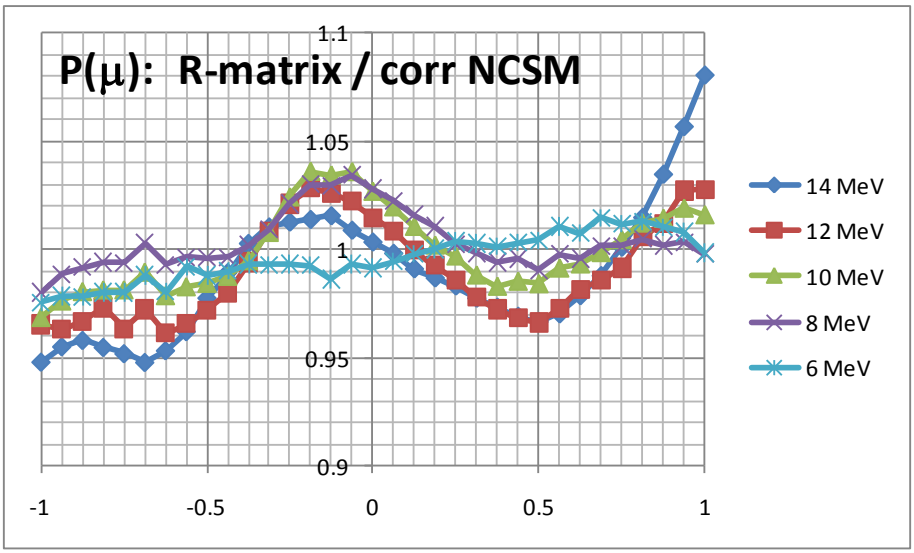


**Figure 7. The ratio of P(μ)s derived from the R-matrix calculations divided by the corrected NCSM/RGM is shown vs. μ=cos $\theta_{cm}$. The complete set is shown in the Appendix, Figure A3.**

Finally, we have performed an average of the present results for the angular distributions, shown in Table 1, with those from the R-matrix calculations as presented in the ENDF/B-VII evaluation. These results are shown in Table 2 in the Appendix. The average was calculated using equal weighting for the two data sets. We estimate the resultant uncertainty in the angle-integrated elastic cross sections as ±1.5%. This is based on the fact that the R-matrix and corrected NCSM/RGM agree within 1% for 6-14 MeV, and also the fact that from 6-10 MeV, where there is no non-elastic contribution, both agree with the measured total cross section to ±1.5%. The angular shapes between the two

distinctly different and independent calculations disagree by up to 5%. We believe that the average of the two calculations is a reasonable estimate of the true value, and so assume that the error on our final averaged P($\mu$)'s does not exceed ±2.5%. Note that if we combine these errors, the uncertainty in the cross section for any point in the differential cross section is then equal to or less than ±3%.

## IV. Discussion

If we compare the integrated elastic cross sections from the R-matrix and corrected NCSM/RGM calculations we find a difference of less than 1%. This is rather spectacular agreement, so we ask why this should be so. First, the correction factor (CF) adds only about 10% to the cross section, so on the average the CF's need only be accurate to 10% to yield this result. Also regarding sensitivity to the CF's, it is only the forward-angle part of the CF's that are important because over half of the integrated cross section lies between $\mu$=0.5 and 1 (*i. e.*, $0^o$ to $60^o$). Our forward-angle CF's do not vary by more than 2%, so our CF's do not alter the integrated cross section by more than 1%. This means that the 100% increase in cross section as the energy descends from 14 to 6 MeV is correctly predicted at the 1% level by both theories. We say this based on experimental n+T total cross sections, which below 8 MeV must be equal to the angle-integrated elastic since no non-elastic channels are open. Even above 8 MeV we believe the non-elastic cross section is small at least up to 12-14 MeV, although this matter has not been definitively settled experimentally. So if the integrated cross sections agree to 1%, why do the angular distributions, as represented by the probability functions P($\mu$), disagree by upwards of 3-4%?

We now look closely at Figure 5. The CF's are all equal around $\mu$ = -0.1 so the structure shown in this region for 8-14 MeV in Figure 7 cannot come from our choice of CF's. Also at 14 MeV the 0.95 ratio at 180° in Figure 7 cannot be due to our choice of CF's since we have high quality p+$^3$He data with which to compare and it would take an energy shift of 2 MeV to produce so large an effect, which is unrealistic. The same is true for the peak at zero degrees for 12 and 14 MeV data (see Figure 7 near $\mu$=1). The only feature in the comparison of P($\mu$)'s shown in Figure 7 that might come from our CF's is the minimum near $\mu$ = 0.5 at the higher energies. Part of this could possibly be explained by a Coulomb-induced angular shift between the n+T angular distribution and our 13.6- and 16.23 MeV p+$^3$He comparison data sets, which were used to determine the n+T correction factor as shown in Figure 2.

It seems realistic to ascribe differences in the angular distributions, as shown by a comparison of the P($\mu$)'s, to essential differences in the two theoretical calculations. Since Hale's R-matrix

calculations are “data driven” (*i.e*., phenomenological) and the NCSM/RGM calculations of Quaglioni and Navratil [2] are based on an “ab initio” shell model theory, such differences are not surprising. What is surprising is their agreement on the integral cross section (after adjustment of the NCSM/RGM calculations via the CF’s). At 14 MeV, the previously attained good agreement was not surprising since both treatments were effectively normalized to the high quality p+$^{3}$He experimental data available at 13.6 and 16.2 MeV. However, there are no similar high quality data sets in the lower energy region.

## V. Conclusions

From the viewpoint of nuclear data applications, the most significant observation is that if ±5% accuracy in the differential cross sections is adequate for NIF diagnostics, then Hale's R-matrix data beyond a c.m. scattering angle of 20° at 14 MeV already achieves the desired accuracy. Hale's data are already available in the current ENDL library. Note that the new 14-MeV data with the CF's generated in this report are within the errors quoted in the report of Navratil *et al*. [1]. However, the difference between the R-matrix and corrected NCSM/RGM results at back angles is reduced by approximately 5% in the present treatment. Combining the results of the present work with the R-matrix calculations has the potential to significantly reduce the uncertainties below the 5% level over the entire energy range.

The averaging of the two calculations gives an error of ±2.5% or less for the whole energy range of 6 – 14MeV and the angular range 30 - 180°. Because of the strong constraint provided by the well-measured total cross section, in principle this should be done by averaging the P(μ) rather than the differential cross sections. However, since the angle-integrated elastic cross sections for the two calculations agree to approximately 1% or better, this distinction is rather unimportant, and the averaged differential cross sections of Table 2 can be taken as a reasonable evaluation of the n+T angular distribution.

The most important physics point is that the differences in angular distribution represent real differences in the calculation of n+T cross sections. In view of this, it is surprising that there is such close agreement between the integrated cross section results over a relatively large (*i. e.*, more than a factor of two) variation in incident energy.

Computer files of the results of this work, including the average of the two calculations, are available on request from one of the authors (T. Luu).

## Acknowledgments

We appreciate the encouragement and support of Dr. R. Fortner and the NIF program at Lawrence Livermore National Laboratory, as well as useful conversations with Prof. S. M. Grimes of Ohio University. TL thanks B. Beck for his help in extracting the ENDF/B-VII data. This work was performed under the auspices of the U.S. Department of Energy by Lawrence Livermore National Laboratory under Contract DE-AC52-07NA27344.

## Appendix

The appendix contains three tables that list various angle-integrated cross sections for neutron scattering on tritium, our newly calculated differential cross sections based on the NCSM/RGM calculations with corrections, and an average of the differential cross sections from the new results and the R-matrix evaluation.

Table 1 lists our calculated estimates of the n+T elastic scattering cross sections for 6 – 14 MeV.

Table 2 lists the average of the corrected NCSM/RGM angular distributions and those from the R-matrix calculations, as described in Section III.

In Table 3 we show a comparison of angle-integrated elastic cross sections and total cross sections. The total cross sections were extracted, using EXFOR, from the ENDF-B/VII file authored by Hale. Hale's integrated elastic angular distribution data is also listed. The difference between these two sets of numbers is Hale's estimate of the nonelastic cross section. Also listed is the integrated elastic cross section from the NCSM/RGM calculations after applying the estimate of the appropriate correction factor (CF) as described in this report. The final column lists the ratio of the cross section values obtained from the R-matrix treatment to those from the corrected NCSM/RGM.

Also included are three figures. The first (Figure A1) is an estimate of the correction factors (CF) for the NCSM/RGM calculations, showing results for neutron energies of 6-14 MeV in 1-MeV steps. This is the same as Figure 5 of the text except all the data is now included in one plot. The second figure (Figure A2) includes all our newly calculated n+T cross sections plotted versus energy and c.m. scattering angle, and is the same as Figure 6 except that all the data from 6 to 14 MeV is now included.

The third figure, (Figure A3), is the ratio of $P(\mu)$ for the R-matrix calculation to that for the corrected NCSM/RGM calculation, where again the full set of data is plotted for the neutron energies between 6 and 14 MeV. This is the same as Figure 7 of the text except that the plot now includes all energies.

Table 1. Elastic differential cross sections for n+T calculated using the corrected NCSM/RGM technique from 6 to 14 MeV laboratory neutron energy. The first column is the c.m. scattering angle in degrees, and the remaining columns are the c.m. differential cross sections in mb/sr.

| Theta | 6 MeV | 7 MeV | 8 MeV | 9 MeV | 10 MeV | 11 MeV | 12 MeV | 13 MeV | 14 MeV |
|---|---|---|---|---|---|---|---|---|---|
| **0.00** | 471.89 | 451.72 | 418.61 | 385.09 | 353.33 | 327.75 | 306.71 | 285.89 | 269.00 |
| **20.36** | 428.72 | 411.45 | 382.15 | 352.43 | 322.45 | 299.36 | 278.92 | 261.05 | 245.09 |
| **28.96** | 389.38 | 374.66 | 348.93 | 321.06 | 294.19 | 273.37 | 254.76 | 238.17 | 223.26 |
| **35.66** | 353.56 | 339.60 | 317.05 | 292.20 | 268.09 | 249.20 | 232.09 | 216.89 | 203.05 |
| **41.41** | 319.13 | 307.09 | 287.36 | 265.18 | 243.57 | 226.52 | 210.91 | 196.71 | 183.43 |
| **46.57** | 287.17 | 277.04 | 259.53 | 239.76 | 221.21 | 204.97 | 190.76 | 177.71 | 165.31 |
| **51.32** | 257.78 | 248.51 | 233.31 | 215.83 | 198.40 | 184.60 | 170.31 | 159.50 | 148.00 |
| **55.77** | 229.28 | 221.90 | 208.35 | 192.99 | 177.47 | 165.27 | 153.35 | 142.03 | 131.89 |
| **60.00** | 203.17 | 196.68 | 184.97 | 171.30 | 157.69 | 146.66 | 135.63 | 125.43 | 116.41 |
| **64.06** | 178.49 | 172.80 | 162.45 | 150.65 | 138.98 | 129.40 | 118.72 | 109.82 | 101.51 |
| **67.98** | 155.83 | 149.42 | 141.07 | 130.96 | 120.85 | 111.50 | 102.92 | 95.04 | 87.76 |
| **71.79** | 134.61 | 129.30 | 121.35 | 112.49 | 103.84 | 95.72 | 88.35 | 81.47 | 75.28 |
| **75.52** | 115.51 | 110.23 | 103.44 | 95.47 | 88.03 | 81.22 | 74.91 | 69.10 | 63.89 |
| **79.19** | 98.89 | 93.52 | 86.96 | 80.39 | 74.11 | 68.32 | 62.92 | 58.17 | 53.76 |
| **82.82** | 84.16 | 78.55 | 72.57 | 66.76 | 61.43 | 56.57 | 52.19 | 48.27 | 44.69 |
| **86.42** | 71.57 | 65.54 | 59.94 | 54.78 | 50.28 | 46.23 | 42.63 | 39.45 | 36.54 |
| **90.00** | 61.05 | 54.58 | 49.19 | 44.61 | 40.72 | 37.35 | 34.42 | 31.82 | 29.50 |
| **93.58** | 52.47 | 45.54 | 40.25 | 36.04 | 32.59 | 29.77 | 27.37 | 25.50 | 23.44 |
| **97.18** | 46.61 | 39.03 | 33.53 | 29.40 | 26.22 | 23.62 | 21.58 | 19.85 | 18.33 |
| **100.81** | 42.45 | 34.18 | 28.42 | 24.27 | 21.18 | 18.79 | 16.98 | 15.50 | 14.30 |
| **104.48** | 40.99 | 31.74 | 25.44 | 21.02 | 17.84 | 15.45 | 13.66 | 12.26 | 11.17 |
| **108.21** | 42.04 | 31.57 | 24.47 | 19.53 | 16.04 | 13.44 | 11.54 | 10.28 | 8.99 |
| **112.02** | 45.62 | 33.62 | 25.45 | 19.78 | 15.78 | 12.83 | 10.67 | 9.02 | 7.81 |
| **115.94** | 52.02 | 38.20 | 28.59 | 21.93 | 17.15 | 13.70 | 11.14 | 9.21 | 7.72 |
| **120.00** | 61.14 | 45.09 | 33.90 | 26.01 | 20.33 | 16.15 | 13.02 | 10.63 | 8.78 |
| **124.23** | 72.67 | 54.66 | 41.60 | 32.29 | 25.46 | 20.63 | 16.52 | 13.53 | 11.18 |
| **128.68** | 88.43 | 67.28 | 52.05 | 40.99 | 32.82 | 26.58 | 21.78 | 18.02 | 15.02 |
| **133.43** | 105.58 | 81.80 | 64.40 | 51.57 | 41.91 | 34.46 | 28.60 | 23.97 | 20.53 |
| **138.59** | 127.61 | 100.56 | 80.85 | 65.78 | 54.28 | 45.29 | 38.17 | 32.38 | 27.74 |
| **144.34** | 152.10 | 122.32 | 99.76 | 82.47 | 69.05 | 58.37 | 49.44 | 42.87 | 37.13 |
| **151.04** | 180.49 | 147.80 | 122.24 | 102.55 | 86.89 | 74.42 | 64.28 | 55.95 | 49.02 |
| **159.64** | 212.13 | 176.62 | 148.49 | 126.12 | 108.50 | 94.03 | 82.28 | 72.50 | 64.27 |
| **180.00** | 248.40 | 210.62 | 179.65 | 154.48 | 134.49 | 117.85 | 103.46 | 93.24 | 83.60 |

Table 2. Elastic differential cross sections for n+T calculated using the average of the corrected NCSM/RGM technique (Table 1) and the current ENDF/B-VII evaluation from 6 to 14 MeV laboratory neutron energy. The first column is the c.m. scattering angle in degrees, and the remaining columns are the c.m. differential cross sections in mb/sr.

| Theta | 6 MeV | 7 MeV | 8 MeV | 9 MeV | 10 MeV | 11 MeV | 12 MeV | 13 MeV | 14 MeV |
|---|---|---|---|---|---|---|---|---|---|
| **0.00** | 476.01 | 451.19 | 416.51 | 386.33 | 355.59 | 333.00 | 312.54 | 294.18 | 279.93 |
| **20.36** | 434.17 | 412.22 | 380.97 | 353.57 | 324.61 | 303.56 | 283.55 | 266.48 | 252.15 |
| **28.96** | 395.13 | 375.81 | 347.84 | 322.28 | 295.82 | 276.35 | 257.59 | 241.23 | 227.23 |
| **35.66** | 358.80 | 341.14 | 316.21 | 293.08 | 268.98 | 251.01 | 233.47 | 218.08 | 204.64 |
| **41.41** | 324.08 | 308.58 | 286.44 | 265.58 | 243.74 | 227.27 | 211.05 | 196.55 | 183.61 |
| **46.57** | 291.53 | 278.10 | 258.38 | 239.64 | 220.32 | 204.89 | 190.00 | 176.55 | 164.39 |
| **51.32** | 261.21 | 249.23 | 231.90 | 215.20 | 197.42 | 183.87 | 169.58 | 157.80 | 146.50 |
| **55.77** | 232.30 | 222.19 | 206.84 | 192.05 | 176.18 | 164.08 | 151.65 | 140.17 | 130.00 |
| **60.00** | 205.54 | 196.70 | 183.33 | 170.20 | 156.20 | 145.33 | 134.01 | 123.66 | 114.53 |
| **64.06** | 180.46 | 172.74 | 161.02 | 149.59 | 137.43 | 127.90 | 117.41 | 108.29 | 99.99 |
| **67.98** | 157.39 | 149.93 | 140.08 | 130.20 | 119.63 | 110.81 | 102.00 | 93.94 | 86.63 |
| **71.79** | 136.07 | 129.66 | 120.78 | 112.16 | 103.06 | 95.42 | 87.81 | 80.78 | 74.47 |
| **75.52** | 116.82 | 110.81 | 103.17 | 95.58 | 87.77 | 81.29 | 74.76 | 68.76 | 63.38 |
| **79.19** | 99.84 | 94.06 | 87.08 | 80.69 | 74.07 | 68.57 | 63.00 | 58.00 | 53.44 |
| **82.82** | 84.86 | 79.12 | 72.86 | 67.27 | 61.66 | 57.04 | 52.44 | 48.28 | 44.51 |
| **86.42** | 72.04 | 66.12 | 60.37 | 55.43 | 50.69 | 46.83 | 43.02 | 39.61 | 36.52 |
| **90.00** | 61.36 | 55.14 | 49.68 | 45.29 | 41.20 | 37.97 | 34.85 | 32.06 | 29.56 |
| **93.58** | 52.79 | 46.11 | 40.78 | 36.72 | 33.12 | 30.40 | 27.82 | 25.67 | 23.56 |
| **97.18** | 46.72 | 39.38 | 33.88 | 29.92 | 26.63 | 24.16 | 21.98 | 20.11 | 18.48 |
| **100.81** | 42.70 | 34.54 | 28.73 | 24.70 | 21.52 | 19.24 | 17.30 | 15.72 | 14.41 |
| **104.48** | 41.24 | 32.01 | 25.60 | 21.28 | 18.03 | 15.73 | 13.87 | 12.41 | 11.25 |
| **108.21** | 42.29 | 31.73 | 24.48 | 19.64 | 16.08 | 13.59 | 11.65 | 10.27 | 9.04 |
| **112.02** | 45.90 | 33.74 | 25.37 | 19.78 | 15.71 | 12.87 | 10.69 | 9.05 | 7.83 |
| **115.94** | 52.25 | 38.21 | 28.43 | 21.85 | 17.02 | 13.66 | 11.08 | 9.15 | 7.69 |
| **120.00** | 61.34 | 45.12 | 33.70 | 25.91 | 20.14 | 16.06 | 12.90 | 10.51 | 8.68 |
| **124.23** | 73.07 | 54.68 | 41.37 | 32.15 | 25.20 | 20.35 | 16.32 | 13.31 | 10.98 |
| **128.68** | 88.38 | 67.14 | 51.66 | 40.75 | 32.42 | 26.32 | 21.47 | 17.66 | 14.68 |
| **133.43** | 105.93 | 82.00 | 64.23 | 51.53 | 41.62 | 34.30 | 28.35 | 23.61 | 20.01 |
| **138.59** | 127.53 | 100.50 | 80.29 | 65.45 | 53.69 | 44.90 | 37.66 | 31.78 | 27.09 |
| **144.34** | 152.01 | 122.10 | 99.07 | 82.03 | 68.30 | 57.90 | 49.02 | 42.10 | 36.31 |
| **151.04** | 180.18 | 147.23 | 121.25 | 101.86 | 85.91 | 73.80 | 63.52 | 55.01 | 48.02 |
| **159.64** | 211.82 | 175.85 | 147.06 | 125.13 | 107.05 | 93.10 | 81.17 | 71.17 | 62.87 |
| **180.00** | 247.66 | 208.94 | 177.18 | 152.63 | 132.17 | 116.31 | 102.17 | 91.17 | 81.47 |

Table 3. Total and angle-integrated elastic cross sections (in millibarns) from various sources.

| Neutron Energy (MeV) | Expt. Total Cross Sections* | Total Cross Sections, R-matrix (ENDF/B-VII) | Integrated Elastic, R-matrix (ENDF/B-VII) | Integrated Elastic, Corrected NCSM/RGM | Ratio of R-matrix To Corrected NCSM/RGM |
|---|---|---|---|---|---|
| 6 | 2029±7 | 2008 | 2008 | 1983 | 1.013 |
| 7 | 1828 | 1800 | 1800 | 1811 | 0.994 |
| 8 | 1659 | 1618 | 1618 | 1636 | 0.989 |
| 9 | 1489 | 1463 | 1461 | 1475 | 0.991 |
| 10 | 1353 | 1331 | 1325 | 1331 | 0.995 |
| 11 | 1233±9 | 1215 | 1209 | 1216 | 0.994 |
| 12 | 1150 | 1115 | 1107 | 1105 | 1.002 |
| 13 | 1066 | 1027 | 1018 | 1018 | 1.000 |
| 14 | 990±15 | 951 | 941 | 947 | 0.994 |

* Ref. [10]. A cubic fit to the Linac data was used from 10 – 14MeV. Sample uncertainties are shown.

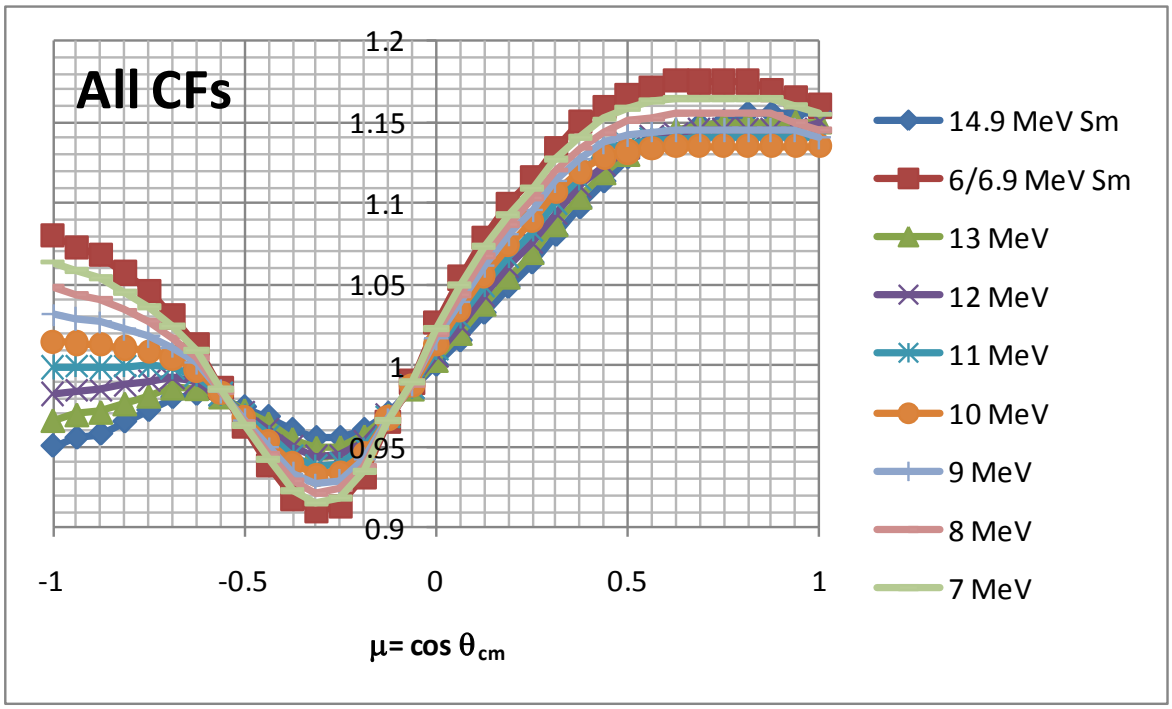


**Figure A1. Same as Figure 5, but showing all energies.**

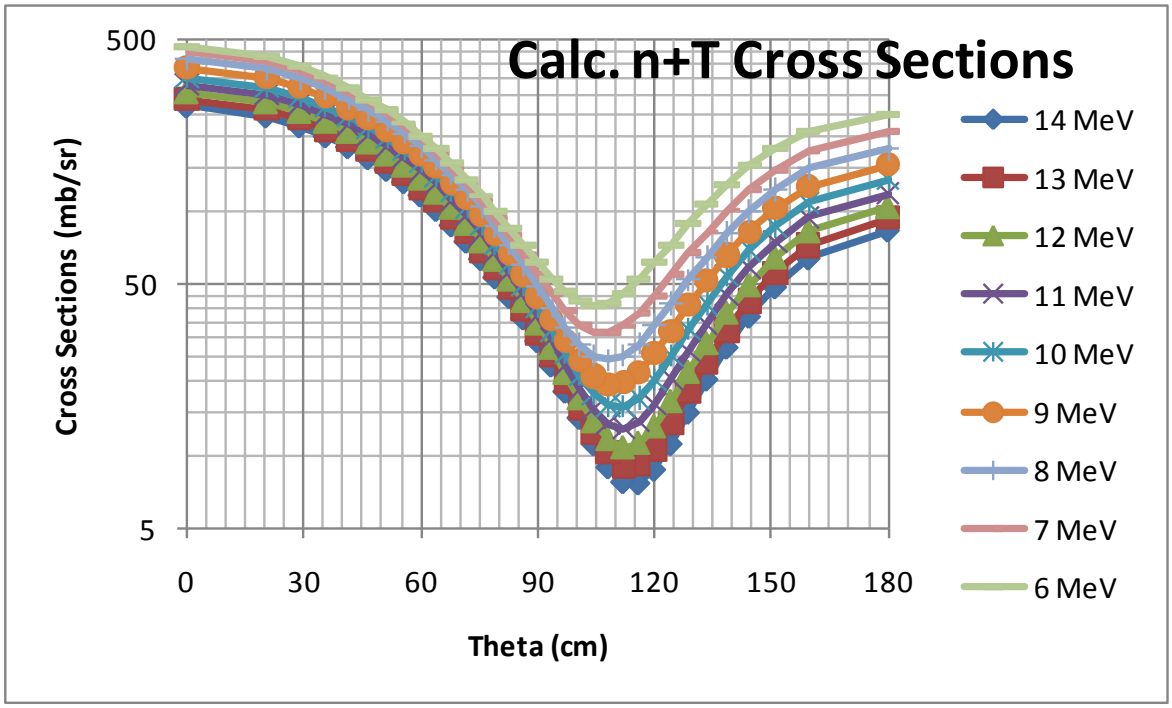


**Figure A2. Same as Figure 6, but showing all energies.**

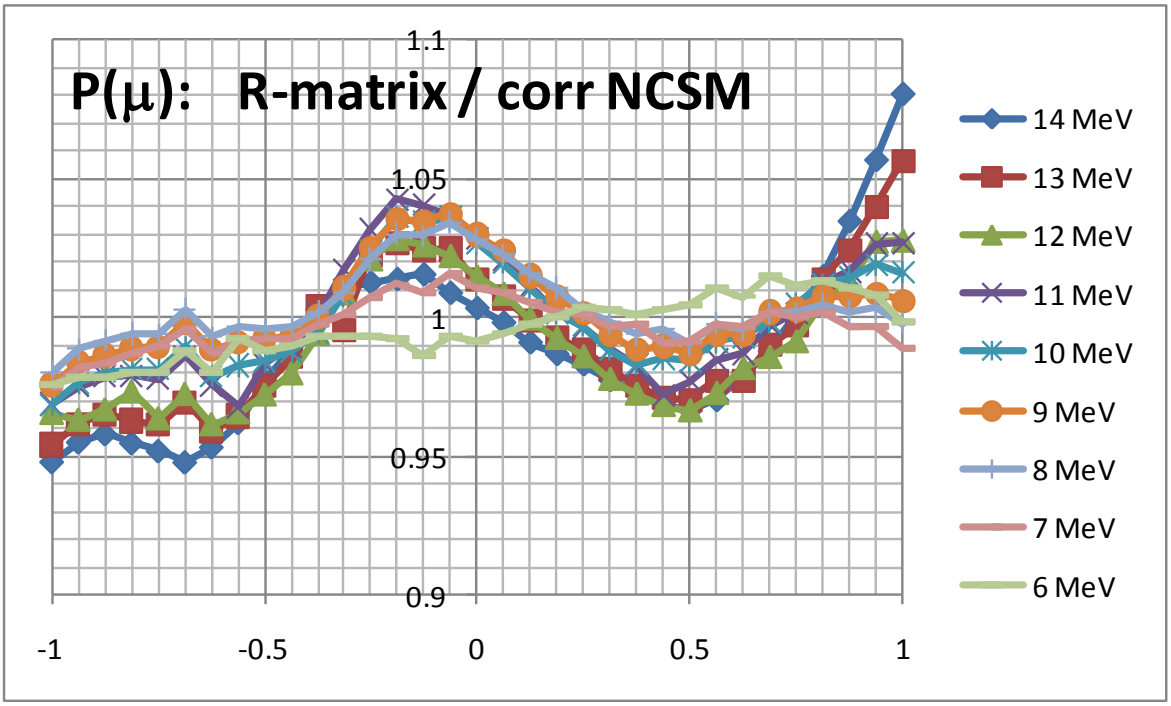


**Figure A3. Same as Figure 7, but showing all energies.**

## References


1. P. Navratil, S. Quaglioni, J. D. Anderson, F. S. Dietrich, D. P. McNabb, and G. M. Hale, Lawrence Livermore National Laboratory Technical Report LLNL-TR-423504 (2010).

2. S. Quaglioni and P. Navratil, Phys. Rev. Lett. 101, 092501 (2008); S. Quaglioni and P. Navratil, Phys. Rev. C **79**, 044606 (2009).

3. G. M. Hale, D. C. Dodder, J. D. Seagrave, B. L. Berman, and T. W. Phillips, Phys. Rev. C **42**, 438 (1990); also see description in ENDF/B-VII database (http://www.nndc.bnl.gov).

4. J. D. Anderson and H. F. Lutz, Lawrence Radiation Laboratory Technical Report UCRL-14955 (1966).

5. R. L. Hutson, N. Jarmie, J. L. Detch, and J. H. Jett, Phys. Rev. C **4**, 17 (1971).

6. D. G. McDonald, W. Haeberli, and L. W. Morrow, Phys. Rev. **133**, B1178 (1964).

7. M. Viviani, A. Kievsky, L. Girlanda, and L. E. Marcucci, Few Body Syst. **45**, 119 (2009).

8. T. B. Clegg, A. C. L. Barnard, J. B. Swint, and J. L. Weil, Nucl. Phys. **50**, 621 (1964).

9. M. P. Nakada, J. D. Anderson, C. C. Gardner, and C. Wong, Phys. Rev. **110**, 1439 (1958).

10. T. W. Phillips, B. L. Berman, and J. D. Seagrave, Phys. Rev. C **22**, 384 (1980).